Regional climate model simulation of precipitation in central Asia: Mean and interannual variability

Eric E. Small[1]

Earth Sciences Department, University of California Santa Cruz

Filippo Giorgi

National Center for Atmospheric Research, Boulder, Colorado

Lisa Cirbus Sloan

Earth Sciences Department, University of California Santa Cruz

Abstract. We examine how well the National Center for Atmospheric Research (NCAR) regional climate model (RegCM2) simulates the mean and interannual variability of precipitation in a semiarid region to more fully establish the strengths and weaknesses of the model as a tool for studying regional scale climate processes. We compare precipitation observations with RegCM2 output from a 5.5 year long simulation of the climate of central Asia, driven by the European Centre for Medium-Range Weather Forecasts analyses. RegCM2 simulates well the spatial patterns and annual cycles of precipitation observed in climatically different subregions. The magnitude of simulated precipitation is similar to observations except over the driest part of Central Asia where the simulated precipitation is too high. We calculate precipitation anomalies for each month as the difference between the monthly total and the 5 year average for that month, from both observations and RegCM2 output. The magnitude of simulated interannual variability is similar to observations, although there are differences. RegCM2 tends to underpredict (overpredict) the magnitude of variability in the same combinations of subregion and season for which it underpredicts (overpredicts) mean precipitation. RegCM2 closely reproduces precipitation anomalies observed in specific months, except during summer and during winter in the mountains. There is no correlation between model biases in mean precipitation and how well the model reproduces a series of precipitation anomalies. This suggests that the processes controlling the mean and the variability of precipitation differ. Therefore evaluating the ability of a regional climate model to simulate both quantities is a demanding test of model performance.

1. Introduction

Regional climate models (RCMs) are useful tools for studying mesoscale climate processes and for identifying the impacts of anthropogenic forcing at the regional scale. However, because these models have been developed only within the last decade, many features of their performance have not been examined in detail. Additional CM evaluation is necessary to establish more fully their strengths and weaknesses.

In this paper, we evaluate how well a RCM simulates (1) the mean precipitation and (2) the interannual variability of precipitation in a semiarid region (central Asia). These two features of RCM performance have not been thoroughly examined in previous studies. We assess these two issues by analyzing a 5.5 year simulation of the present-day climate of central Asia produced with the National Center for

Atmospheric Research (NCAR) regional climate model (RegCM2) driven by observed boundary conditions. The work presented here is part of a larger effort to study climatic change in central Asia. In particular, we are using RegCM2 to examine climatic and hydrologic changes associated with (1) desiccation of the Aral Sea and (2) enhanced greenhouse gases. The performance of this modeling system in simulating surface air temperature and the hydrologic budget of the Aral Sea is evaluated in a companion paper [*Small et al.*, this issue].

RCM experiments of less than several months in duration have been completed for various climatic regimes (reviewed by *McGregor* [1997]), including arid to semiarid environments [e.g., *Semazzi et al.*, 1993; *Jenkins*, 1997]. In these short simulations the RCM has primarily been forced by analyses at the lateral boundaries of the domain. Overall, these studies have shown that RCMs driven by observed boundary conditions reproduce synoptic circulations well and realistically respond to mesoscale forcing; however, significant precipitation biases are common [*Giorgi*, 1995].

Continuous multiyear simulations, which are more useful to evaluate how well RCMs simulate climate, have also been completed. In these experiments the RCM has been driven at the lateral boundaries by either analyses or GCM output.

---

[1]Now at Department of Earth and Environmental Science, New Mexico Tech, Socorro, NM.

Multiyear simulations have been completed for the United States [Giorgi et al., 1993a; Giorgi et al., 1994] eastern Asia and Japan [Hirakuchi and Giorgi, 1995], and Europe [Marinucci and Giorgi, 1992; Jones et al., 1995]. These studies have shown that RCMs reproduce well the observed present-day mean climate when the model is forced by boundary conditions that accurately represent the observed synoptic scale atmospheric conditions.

These previous multiyear experiments have shown that RCMs work well in nonarid regions; however, multiyear integrations of arid or semiarid climates have not been previously reported. Because model parameterizations are tuned to reproduce the mean conditions observed in some area, a skillful reproduction of nonarid region precipitation does not verify that a model can successfully simulate precipitation in more arid environments. Our simulation of the present-day climate of central Asia tests the flexibility of the RegCM2 modeling system. The model domain used here includes extensive arid and semiarid regions, where annual precipitation is less than 15 cm, as well as much wetter areas where annual precipitation exceeds 50 cm. This contrast allows us to address the following question: Are the various components of RegCM2 versatile enough to reproduce both arid and nonarid climates? In particular, this evaluation is a strict test of the parameterizations in the moist physics and land surface schemes.

Whereas previous RCM studies have been focused on mean climate conditions, much less is known about how well RCMs simulate interannual variability. The second goal of this study is to provide a detailed comparison between RCM and observed interannual precipitation variability. This comparison is important for several reasons. First, the degree of similarity between modeled and observed interannual precipitation variability is an important model diagnostic, as it is one way to test the sensitivity of a RCM to a range of synoptic scale atmospheric conditions. Second, year-to-year changes in precipitation have large socioeconomic impacts at the regional scale. Therefore it is critical to evaluate when and where climate anomalies are predictable and to assess the performance of RCMs in reproducing them. Third, the interannual variability of precipitation may change due to anthropogenic increases in atmospheric greenhouse gases. Before we can incorporate RCM predictions of variability changes in impacts assessments, we must first evaluate how well these models simulate present-day variability.

One method to evaluate how well a RCM simulates year-to-year changes in precipitation is to compare the magnitudes of observed and simulated variability (e.g., the standard deviations). This method has at least two drawbacks: (1) Long simulations are needed to yield statistically meaningful results and (2) it is not a rigorous test of whether the RCM responds correctly to a specific set of synoptic scale atmospheric conditions. An alternative approach is to compare the simulated and observed precipitation anomalies for specific months or seasons [Luthi et al., 1996; Jenkins and Barron, 1997; Walsh and McGregor, 1997]. By comparing particular observed anomalies, one can directly test if the RCM has the correct sensitivity to specific forcings. We use both methods in this study.

Luthi et al. [1996] examined how well a RCM forced by analyses reproduced year-to-year precipitation changes over Europe in simulations representing three different Januarys and Julys. They found that the model was able to reproduce interannual variability in January but not in July and that the

quality of simulated variability varied spatially. They suggested the simulations of variability were inferior in July because the model produced larger dynamical errors in this month and because the influence of subgrid scale processes on precipitation is greater during the summer season. In studies with GCM boundary conditions the nested RCM improved the simulation of precipitation anomalies that were associated with particular forcing, compared to the driving GCM [Jenkins and Barron, 1997; Walsh and McGregor, 1997]. However, the simulations examined in these studies were short (only one or two seasons), and there were large model biases in both the RCM and the driving GCM. Similar to the findings of Luthi et al. [1996] the quality of the simulated interannual variability varied spatially.

In this study, we explore the following questions related to how well RegCM2 simulates the observed interannual variability of precipitation in central Asia: (1) How does the simulated magnitude of variability compare to observed values? (2) How does the correlation between observed and simulated anomalies vary spatially and seasonally? (3) What controls whether precipitation anomalies can be predicted by a RCM? (4) How does the model's ability to simulate variability compare to its ability to simulate mean precipitation?

We first describe the details of the model experiment and the observations used to evaluate the model performance (section 2). Next we discuss the synoptic scale controls of central Asian climate and compare the observed mean atmospheric fields European Centre for Medium-Range Weather Forecasts (ECMWF) analyses) to those simulated by RegCM2 (section 3). This is followed by a comparison of the observed and simulated mean precipitation (section 4). We then assess how well RegCM2 simulates the observed interannual variability of precipitation, including the magnitude of variability and the anomalies associated with particular forcing (section 5). In the following section we discuss what the comparison between simulated and observed variability indicates about model performance and the predictability of climate anomalies in central Asia (section 6). Finally, we compare model biases in mean precipitation to the model's performance in simulating interannual variability (section 7).

2. Experimental Design

2.1. Regional Climate Model

In this study, we use a version of NCAR's regional climate model, RegCM2. Because this model is described in detail elsewhere [Giorgi, 1993b,c], we include only a brief description here. The NCAR RegCM was originally developed by Dickinson et al. [1989], Giorgi and Bates [1989], and Giorgi [1990]. It is an augmented version of the NCAR/Pennsylvania State University mesoscale model MM4 [Anthes et al., 1987]. MM4 is a primitive equation, σ vertical coordinate, grid point limited-area model with compressibility and hydrostatic balance. Some of the physics parameterizations that were added to MM4 to improve its suitability for climate studies include (1) the convection parameterizations of Grell [1993]; (2) Holtslag's et al. [1990] non-local formulation of vertical transport in the planetary boundary layer; (3) the NCAR CCM2 radiative transfer package, which explicitly accounts for the effects of CO_2, O_3, H_2O, O_2, and clouds [Bri, 1992]; (4) a simplified explicit cloud water scheme which prognostically calculates precipitation and cloud water for radiation calculations [Giorgi

and Shields, 1998]; and (5) the biosphere-atmosphere transfer scheme (BATS) surface physics package [*Dickinson et al.*, 1993].

To account for the surface fluxes of heat, moisture, and momentum from the Aral and Caspian Seas, we use an inland water model that is interactively coupled to RegCM2 [*Hostetler et al.*, 1993]. This model is an updated version of *Hostetler and Bartlein's* [1990] one-dimensional lake model, in which heat is transferred vertically by convective and eddy mixing. The improvements to this model and its performance for central Asia are described in detail elsewhere [*Small et al.*, this issue]. In this study, the inland water model is used to compute (1) Aral sea surface temperatures (SSTs), (2) Aral and Caspian ice thickness and ice/snow surface temperatures, and (3) surface fluxes from both water bodies. We prescribe Caspian sea surface temperatures (SSTs) because a one-dimensional heat transfer approach is inadequate to represent the complex circulations in the Caspian. When the Caspian SST data indicate water is at or below the freezing point, ice thickness and surface temperature are calculated using the ice scheme of the inland water model.

2.2. Model Domain

The model domain used here has a resolution of 50 km and covers a 3400 x 3100 km^2 area, centered over central Asia. Figure 1 shows the topography and vegetation/land cover for this area. There is a distinct contrast between the topography in the northern and southern portions of the simulation area: Low elevations are dominant throughout the northern two thirds of the domain, whereas elevations greater than 2 km are common in the south. The highest elevations, which are in the southeastern corner, represent the Pamir, Tien Shan, and the northwestern edge of the Himalaya Mountains. Whereas actual peak elevations in these ranges exceed 7.5 km, the highest model elevations at 50 km grid point spacing are ~5 km. BATS land cover categories (Figure 1) were set according to the Olsen 30 min. global ecosystem data set, available in the NCAR data archives. Desert and grassland are the most common land use types, followed by crop. Trees and woodlands are primarily found along the northern boundary of the domain.

We have divided the domain into three subregions: north, central, and mountains/south (Figure 1). The observed climate in each subregion is very different, as discussed below. We use these subregions to compare observations and model output, to assess how well RegCM2 simulates the spatial variability of climate processes across central Asia.

2.3. Boundary and Initial Conditions

RegCM2 was integrated for a continuous ~5.5 year period, from June 1, 1987 to January 1, 1993. Time-dependent lateral boundary conditions for this simulation were taken from the (ECMWF) analyses. In the version of the ECMWF analyses used here, fields are available every 12 hours on a T42 spectral grid [*Trenberth*, 1992]. The fields used as lateral boundary conditions include wind, temperature, water vapor, and surface pressure. They were applied over a 400 km buffer zone along the lateral boundaries of the domain (Figure 1). This was done using the relaxation method of Anthes et al. [1987], modified so that the forcing is stronger at higher model levels and decreases exponentially with distance from the domain boundary [*Giorgi et al.*, 1993c]. Time-dependent Caspian SSTs were taken from the Pathfinder AVHRR SST data set,
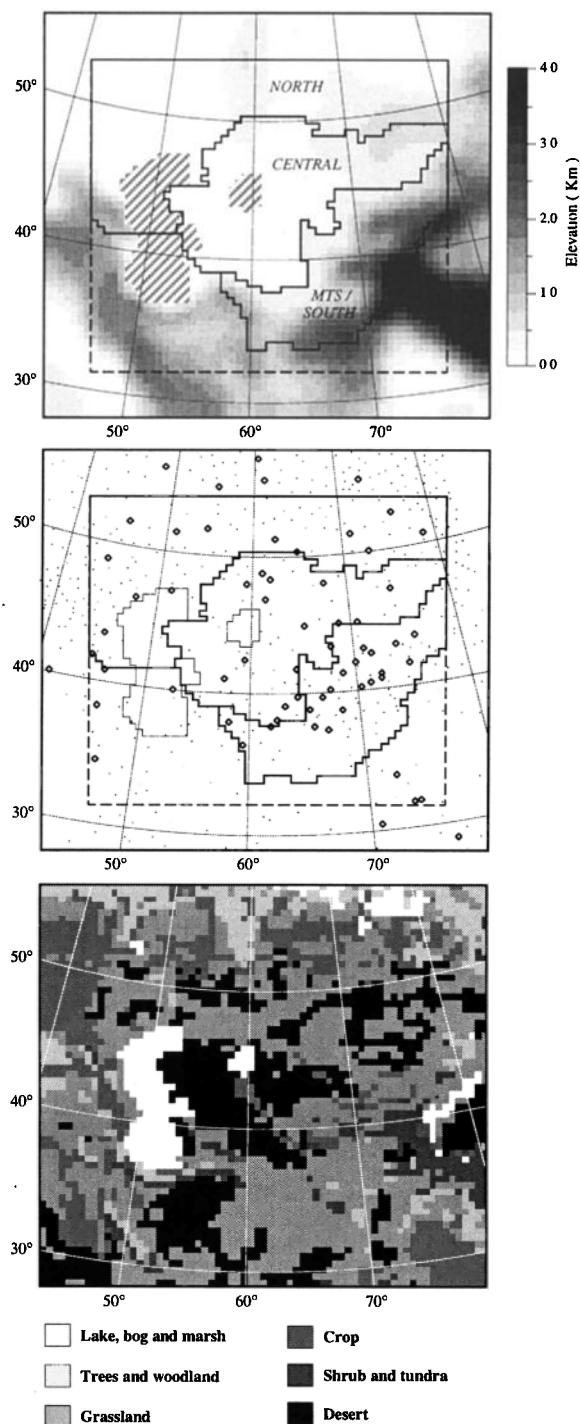

Figure 1. Numbers on outside of maps indicate degrees north latitude and degrees east longitude. (top) Shading depicts surface elevation. The north, central, and mountains or south subregions are defined by solid lines. The solid and dashed rectangle shows the inner edge of the buffer zone throughout which boundary conditions are applied. The Caspian and Aral Seas are hatched. (middle) Dots show location of Climate Analysis Center (CAC) meteorological stations from which temperature measurements were used. Larger open symbols show locations of CAC stations from which precipitation data were used. Dots show location of all CAC stations in the domain. (bottom) Biosphere-atmosphere transfer scheme (BATS) land cover categories for the model domain. Not all 14 BATS categories are shaded differently. Instead, like categories (e.g., tall and short grass) have been shaded similarly.

available from the Physical Oceanography Distributed Active Archive Center (PODAAC) at the Jet Propulsion Laboratory (JPL).

We initialized soil moisture by using results from a previous 5 year simulation completed with the same model domain. Soil moisture in this previous experiment was initialized as a function of land cover, as described by *Giorgi and Bates* [1989]. These soil moisture values were too high for central Asia, and the quantity of water in the entire soil column (3 m) only appeared to reach a steadystate after ~3-4 years of simulation. The soil moisture initialization for the experiment examined here is much improved, as soil moisture did not noticeably drift throughout the simulation. We exclude the first seven months of this simulation (June - December 1987) from all analyses to minimize other possible problems associated with model spin-up. This leaves five complete years (1988-1992) for which we compare model output to observations.

2.4. Observations Used to Assess Model Performance

We use the Legates and Willmott precipitation climatology (LWC) [*Legates and Willmott*, 1990] and a Climate Analysis Center (CAC) monthly data set available in the NCAR archives to evaluate the accuracy of the modeled precipitation. The LWC was constructed by averaging ~60 years of monthly station data (1920-1980). On the basis of empirical relationships, rain gauge type, and local climatic conditions the long-term monthly means from each station were adjusted for losses resulting from wind, gauge wetting, and evaporation from gauges [*Legates and Willmott*, 1990]. Observed and corrected precipitation were then interpolated onto a 0.5° x 0.5° grid. The interpolated precipitation values are possibly unreliable in parts of central Asia where station density is low. We interpolate the observed and corrected LWC precipitation onto the RegCM2 grid. We also use the spatially varying precipitation correction of the LWC for each month (i.e., the difference between the corrected and the observed LWC fields) to estimate biases in the CAC precipitation data set.
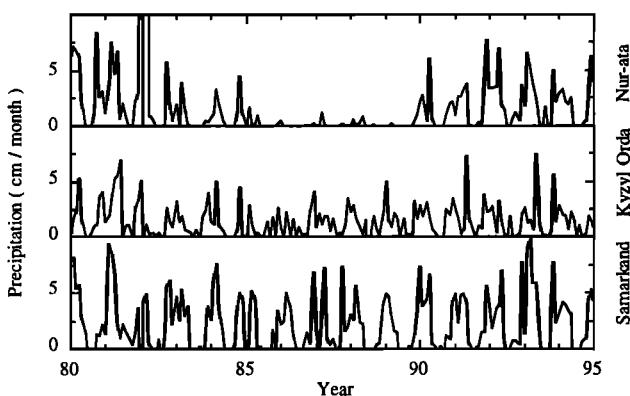

Figure 2. Monthly precipitation (cm) at three central Asian stations included in the CAC data set: (top) Nur-ata, (middle) Kyzyl Orda, and (bottom) Samarkand. Records cover the interval from 1980 to 1995. Stations are within 200 km of each other and at similar elevations. The Nur-ata record is likely incorrect in many months between 1985 and 1990: 0.0 cm precipitation is frequently reported, whereas comparable anomalously dry conditions are not observed at either nearby station.

There are two problems with the CAC monthly precipitation data from stations in central Asia. First, "no-data" flags that indicate bogus 0.0 precipitation values are rarely included in the records for some stations. This makes it difficult to distinguish between months in which no data was reported and months when there was no precipitation (Figure 2). To include only stations with reliable data flags in our analyses, we chose 65 stations, from the ~400 within our model domain (Figure 1), which had visually homogenous monthly precipitation records (Figure 2). The difference between domain-averaged precipitation for all CAC stations and those we selected exceeds 20% in some months. The second problem is that "reported" and "estimated" monthly precipitation values are commonly very different, even for months with no missing daily reports. In all our analyses we use estimated precipitation values and exclude individual months in which reported and estimated precipitation differs by more than 20%. We do not use monthly precipitation values determined from fewer than 25 daily reports.

3. Atmospheric Circulations

In this section, we first describe the observed (ECMWF) mean atmospheric circulation fields over central Asia, including sea level pressure, 500 mbar geopotential height, and the vertically integrated water vapor flux. After describing the observed fields, we evaluate how closely they are reproduced by RegCM2 and discuss how differences could influence the precipitation predicted by the model.

3.1. Observed Circulations

During winter, two features dominate the mean sea level pressure field: (1) the western margin of the thermally induced central Asian (or Siberian) high (CAH) extends roughly halfway across the domain; and (2) an area of low pressure exists in the north, corresponding to the passage of cyclonic storms generated over the Icelandic Low (Figure 3a). Storms generated in the Mediterranean region also influence central Asia, and enter the domain from the southwest corner. A trough in the 500 mbar height field (Figure 4a), which is strongest between November and January, steers Icelandic and Mediterranean storms and their attendant high moisture fluxes (Figure 5a) across the domain from southwest to northeast. The paths of storms are also influenced by the position and intensity of the CAH. The CAH tends to force Icelandic storms to the north or to the south toward the mountains of central Asia [*Lydolph*, 1977]. In addition, year-to-year changes in the position and intensity of the CAH exert a strong influence on whether Mediterranean storms bring moisture to the mountain subregion. When the CAH is relatively weak over the southern part of central Asia, Mediterranean storms are able to track north through the gap in the mountains located between 55°E and 65°E (Figure 1), resulting in a strong northward moisture flux at this location (Figure 5). When the CAH is relatively strong over southern central Asia, Mediterranean storms are not able to cross the mountains from south to north, and this moisture source is cut off.

Spring circulations differ from winter circulations in several ways (1) The CAH is weaker and is centered in the northeast corner of the domain (Figure 3a); (2) the 500 mbar height flow is more zonal, owing to the weakening of the winter season trough (Figure 4a); and (3) the southern moisture source shifts northward and becomes more intense (Figure 5a). The result of
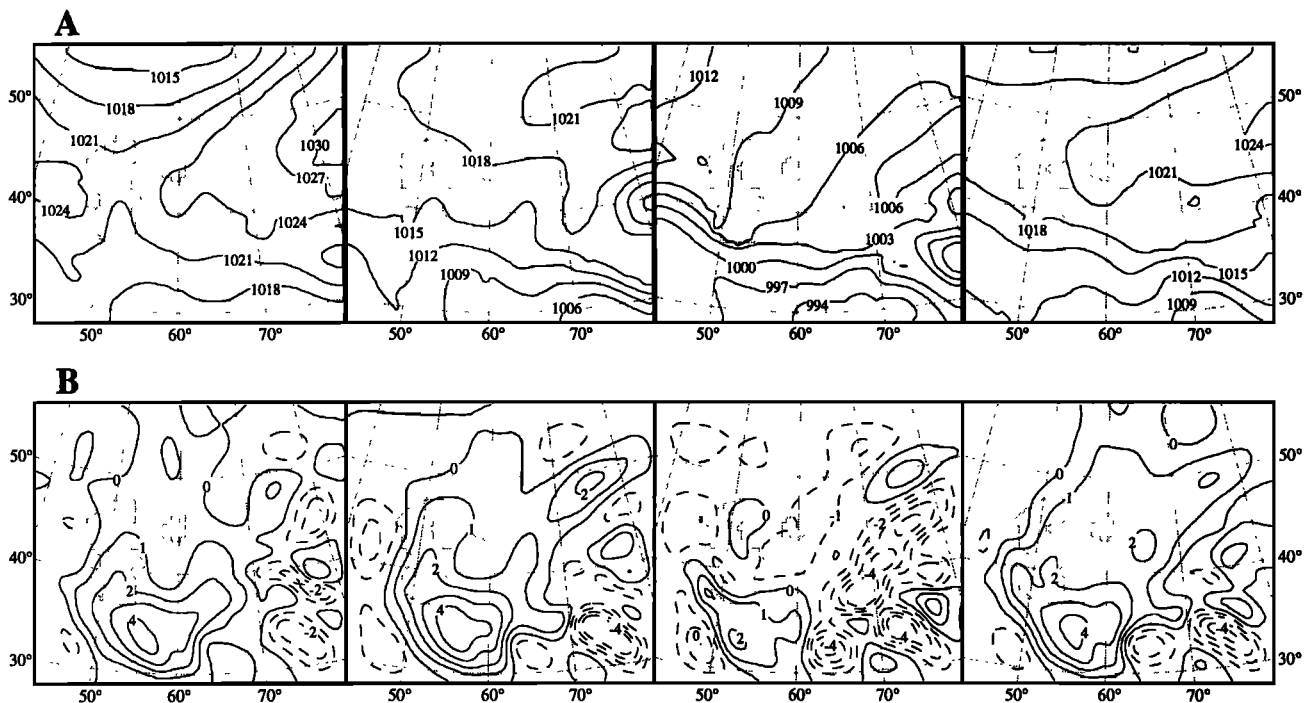
A

B

Figure 3. (a) Maps of European Centre for Medium-Range Weather Forecasts (ECMWF) monthly mean sea level pressure for January, April, July, and October (left to right) in mbar, averaged for the interval 1988-1992. Contour interval is 3 mbar. (b) Difference between RegCM2 and ECMWF monthly mean sea level pressure. Contour interval is 1 mbar.

these changes is that storms from the Mediterranean/Black Sea region travel directly across central Asia. This leads to a maximum in cyclonic storm frequency and precipitation over the central and mountain subregions during spring (Figure 1) [*Lydolph*, 1977]. At the same time, the CAH gives rise to relatively dry conditions farther north.

During summer the southeastern extension of the Azores anticyclone generates high pressure over the northwestern portion of the domain (Figure 3a). This high pressure is enhanced by a local anticyclone that builds over the Caspian Sea at this time of year. Because the 500 mbar height flow is relatively weak (Figure 4a), the surface pressure field has a
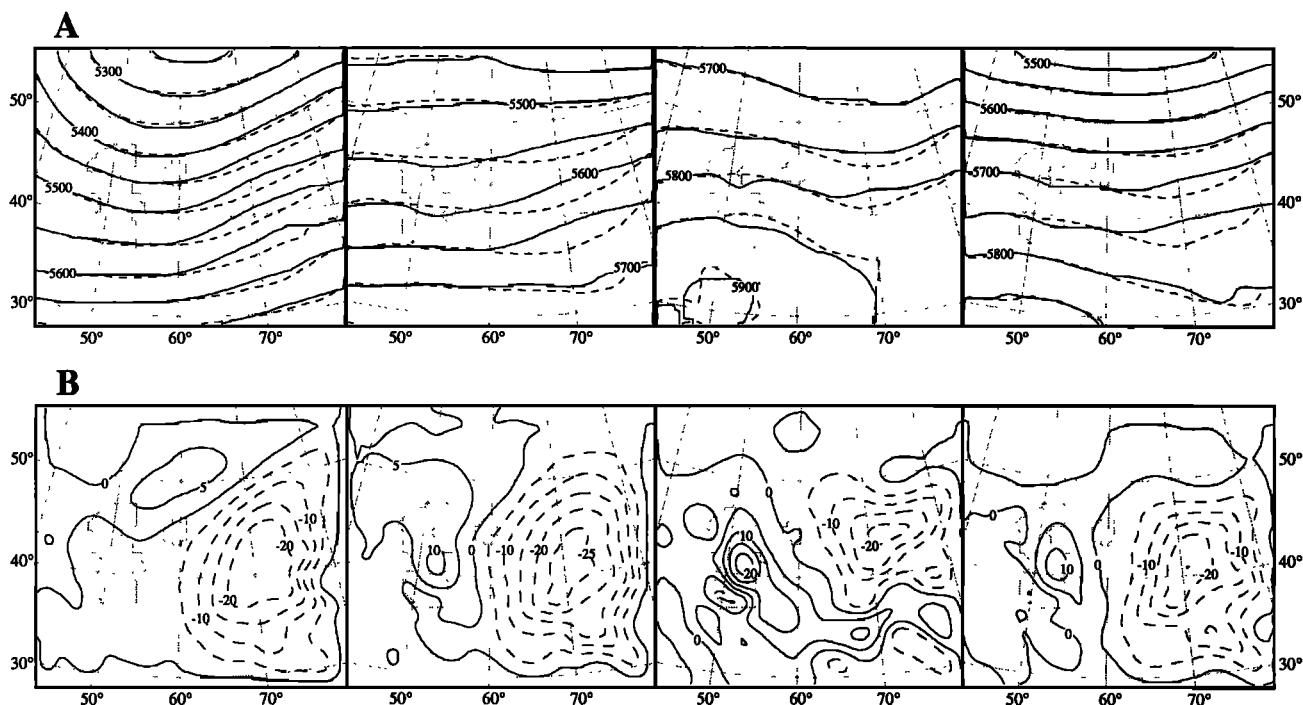
A

B

Figure 4. (a) Maps of ECMWF (solid) and RegCM2 (dashed) 500 mbar geopotential height for January, April, July, and October (left to right) averaged for the interval 1988-1992. Contour interval is 50 m. (b) Difference between RegCM2 and ECMWF 500 mbar geopotential height. Contour interval is 5 m.
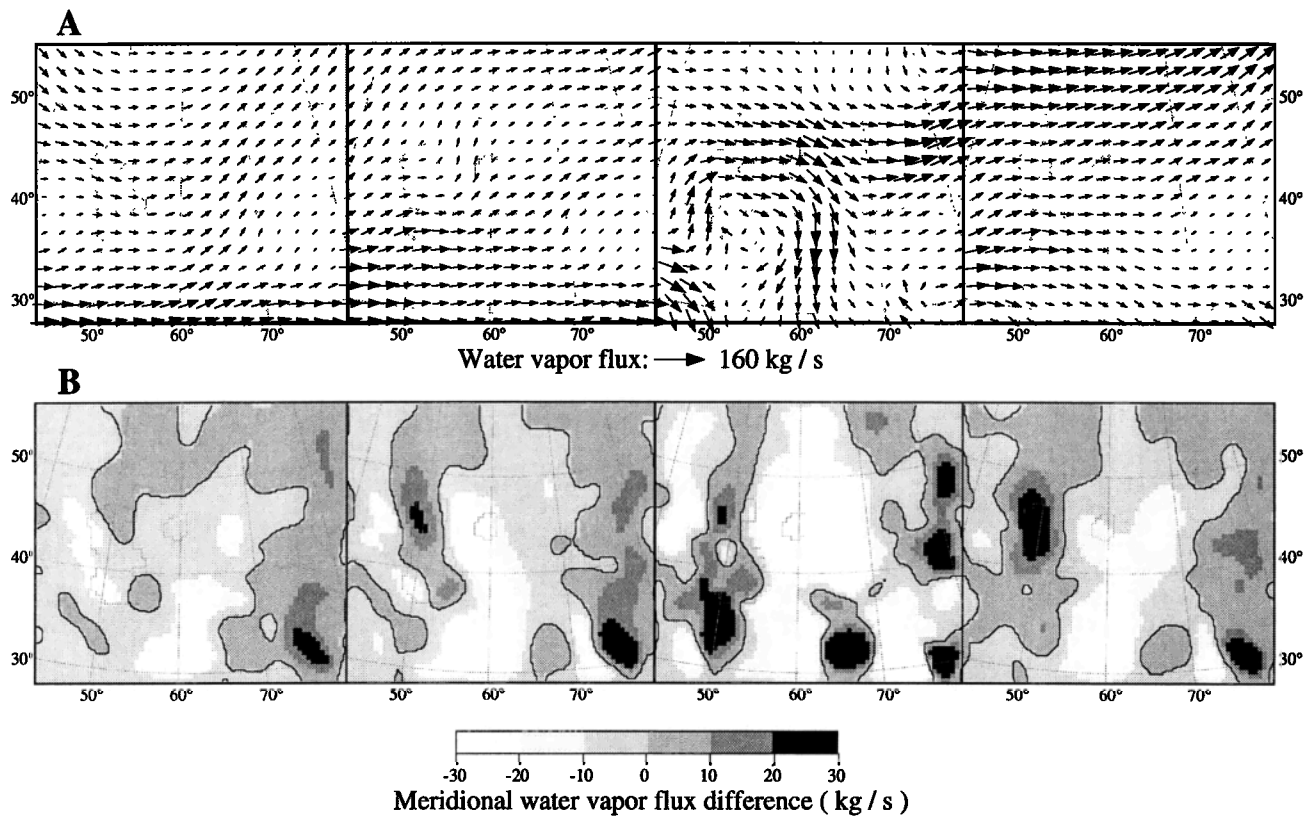
A

Water vapor flux: ➤ 160 kg / s

B

-30   -20   -10   0   10   20   30
Meridional water vapor flux difference (kg / s)

Figure 5. (a) ECMWF vertically integrated water vapor flux for January, April, July, and October (left to right) averaged for the interval 1988-1992. (b) Difference between RegCM2 and ECMWF meridional vertically integrated water vapor flux.

large influence on the direction of water vapor transport, producing a large southward flux across southern central Asia (Figure 5a). The north-south surface pressure gradient and the attendant water vapor flux are enhanced by a thermally induced surface low along the southern boundary of the domain (Figure 3a).

Fall circulations are roughly intermediate between those observed during winter and spring. Whereas the water vapor flux from the North Atlantic is stronger during the fall than in any other season (Figure 5a), it produces little precipitation, except over the northernmost portion of the domain. There are two reasons for this: (1) flow aloft is nearly zonal, especially compared to the winter, so the moisture is not carried south into the domain (Figure 4a); and (2) although the CAH high is not so intense as during the winter months, it is positioned in roughly the same location (Figure 3a). This inhibits precipitation in the central and southern portions of the domain.

3.2.   Simulated Circulations

In all seasons, RegCM2 sea level pressure is within ~1 mbar of ECMWF sea level pressure, throughout low-elevation areas of the domain (Figure 3b). Larger differences exist between RegCM2 and ECMWF sea level pressure in areas of high topography. These differences mostly arise through interpolation from surface to sea level pressure.

More important differences exist between RegCM2 and ECMWF 500 mbar height (Figure 4b). The RegCM2 500 mbar height is too low in the eastern half of the domain in all

seasons, with the greatest bias during the spring. In all seasons but winter, there is also a localized positive bias over the Caspian Sea (Figure 4b). Because RegCM2 and ECMWF surface pressure are nearly identical, the negative (positive) 500 mbar height bias indicates that RegCM2 lower troposphere temperatures are lower (higher) than those in ECMWF analyses. The source of this difference could be related to RegCM2's dynamics or to physical processes such as cloud-radiation interactions. A negative water vapor bias of ~0.5-1.0 g/Kg is associated with the region of lower tropospheric temperatures (not shown). These RegCM2-ECMWF differences are similar to those found in other applications of RegCM2 [e.g., Liu et al., 1996].

The most important effect of the RegCM2 500 mbar height biases is that the meridional component of the 500 mbar height flow is somewhat different from that in the ECMWF analyses. In regions where the ECMWF 500 mbar height meridional flow is northward, negative (positive) zonal gradients in the 500 mbar height bias lead to reduced (increased) northward flow. The opposite occurs when the ECMWF 500 mbar height meridional flow is southward. This relationship produces differences between RegCM2 and ECMWF meridional moisture fluxes (Figure 5b). For example, during spring the 500 mbar height meridional flow and the vertically integrated meridional water vapor flux are northward throughout the domain. During this season, there is also a negative zonal gradient in the 500 mbar height bias from longitude 50° to 70°E (Figure 4b). The result is that the northward water vapor flux in RegCM2 is less than in the ECMWF analysis across the center of the domain (Figure 5b).
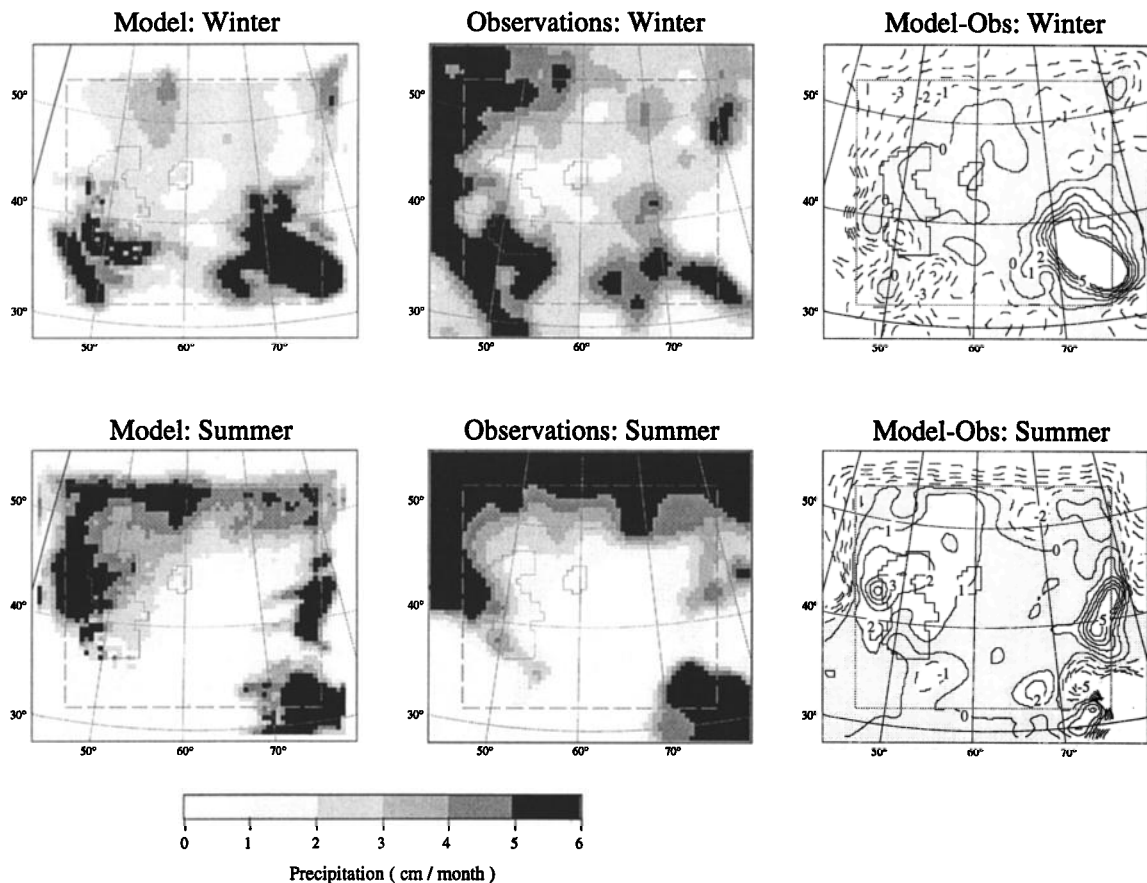
Figure 6. (top) Winter RegCM2 precipitation (left), Legates and Willmott corrected precipitation climatology (LWC) (center), and RegCM2-LWC difference (right). The contour interval is 1 cm/month on the difference maps, and shaded area shows the region in which the absolute value of the difference is less than 1 cm /month. (bottom) Same for summer precipitation.

Along the western and eastern domain boundaries, where the zonal gradient of the 500 mbar height bias is positive, the northward water vapor flux in RegCM2 is greater than in ECMWF. This pattern of reduced RegCM2 meridional flux from longitude 50° to 70°E and enhanced RegCM2 flux along the meridional domain boundaries exists in all seasons and possibly affects precipitation.

4. Mean Precipitation

4.1. Spatial Patterns

We compare simulated precipitation to the Legates and Willmott precipitation climatology in Figure 6. Excluding

the boundary regions, RegCM2 does an adequate job of simulating the relative spatial patterns of precipitation during summer. Simulated precipitation is less than 1 cm/month throughout most of the southern half of the domain, which is in agreement with the climatology. The model also reproduces the high meridional precipitation gradient in the northern third of the domain between 50° and 70°E. In this region, observed precipitation decreases from 6 cm/month to less than 1 cm/month over a distance of ~500 km. It is particularly impressive that the model reproduces this feature because the high precipitation gradient is not topographically induced. The simulated gradient is lower than in the climatology in some areas; however, this could be related to the comparison

Table 1. Simulated and Observed Spatial Standard Deviation (SSD) of Precipitation (cm) for the Entire Domain

	Number of Stations= 52				
	DJF	MAM	JJA	SON	Annual
Model: SSD	1.78	1.67	2.31	1.16	1.27
Observations: SSD	1.71	2.08	2.50	1.11	1.37
Correlation coefficient r	0.67	0.49	0.76	0.67	0.66

Spatial correlation coefficient r calculated between all precipitation stations and corresponding model grid cells.

between a 5 year model average and a long term climatology representing a different time interval. We use CAC precipitation data from 1988 to 1992 to calculate spatial precipitation statistics for the entire model domain excluding the buffer zone. Statistics are calculated over the subset of model grid cells in which meteorological stations with acceptable precipitation records exist (Figure 1, Table 1). The spatial correlation coefficient during summer (0.76) is higher than in any other season. The simulated spatial standard deviation of summertime precipitation closely matches the observed.

During winter, RegCM2 reproduces the climatological precipitation patterns (Figure 6) in areas distant from the inflow boundaries (Figure 5). For example, both the minimum around the Aral Sea and the maxima over high-elevation regions are simulated well. The gridded LWC was constructed with few or no meteorological stations in the southeastern, high-elevation portion of the domain [*Legates and Willmott*, 1990]. The interpolation of precipitation across this region is probably an important source of the model-climatology differences that exist in this area. Closer to the inflow at the NW and SW corners of the domain (Figure 5), RegCM2 does a poorer job of reproducing the wintertime precipitation patterns in the LWC. The greatest difference is in the northwest corner of the domain. In this area the observed precipitation decreases from northwest to southeast, as midlatitude storms weaken along their trajectories. In contrast, the simulated precipitation increases toward the southeast and east. This difference in the sign of the precipitation gradient extends ~750 km from the northwest corner of the buffer zone. This error is probably related to how RegCM2 assimilates the inflow of water vapor at this location. Before precipitation forms in RegCM2, the condensation of water vapor must raise the mixing ratio of cloud water above a temperature-dependent threshold, and the mixing ratio of cloud water is set to zero at the domain boundaries. Therefore it takes some time for the convergence associated with cyclonic storms to raise cloud water amounts above the threshold and produce precipitation, within inflow portions of the buffer zone. In the NW corner of the domain, precipitation is probably too low because the cloud water mixing ratio has not grown fast enough from the specified zero value at the domain boundary. A similar problem should exist in any RCM that does not assimilate but explicitly represents cloud water. Solutions to this problem include (1) increasing domain size so that edge effects are minimized or (2) assimilating cloud water at the domain boundaries. The second solution is possible only if cloud water is available in the data from which boundary conditions are derived, which is typically not the case for analyses.

The pattern mismatch at the inflow boundary also exists between the model and the CAC data, as evidenced by a lower wintertime pattern correlation coefficient (0.67) than during summer. Even with the problems at the inflow boundary, the precipitation pattern is still simulated better during winter than during spring, when the correlation coefficient is only 0.49. During spring, the simulated precipitation over the mountains in the southeastern portion of the domain is too low. This reduces the simulated spatial standard deviation, leading to the greatest seasonal difference between simulated and observed values of spatial variability (Table 1). During fall the quality of the simulated precipitation pattern is similar to winter.

4.2. Annual Cycle and Magnitude of Precipitation

To compare the shape of simulated and observed annual cycles of precipitation for each subregion, we calculate means over the model grid cells in which CAC meteorological stations with acceptable precipitation records exist (Figure 7, Table 2). Compared to the CAC data averaged over the same 5 year interval, RegCM2 simulates the shape of the annual cycle of precipitation well in each subregion. In the north the model reproduces the July maximum as well as the February-March minimum. Compared to the northern subregion, the amplitude of the annual cycle is much smaller in the central region. RegCM2 reproduces this difference, as well as the timing of the precipitation peaks in December-January and May. In the mountains the amplitude of the annual cycle and the timing of the summer minimum and December maximum are simulated well by the model. However, the model fails to simulate the observed peak during spring. The subregion-averaged annual cycles in the LWC are similar to those from the CAC data set, except in the north where the amplitude of
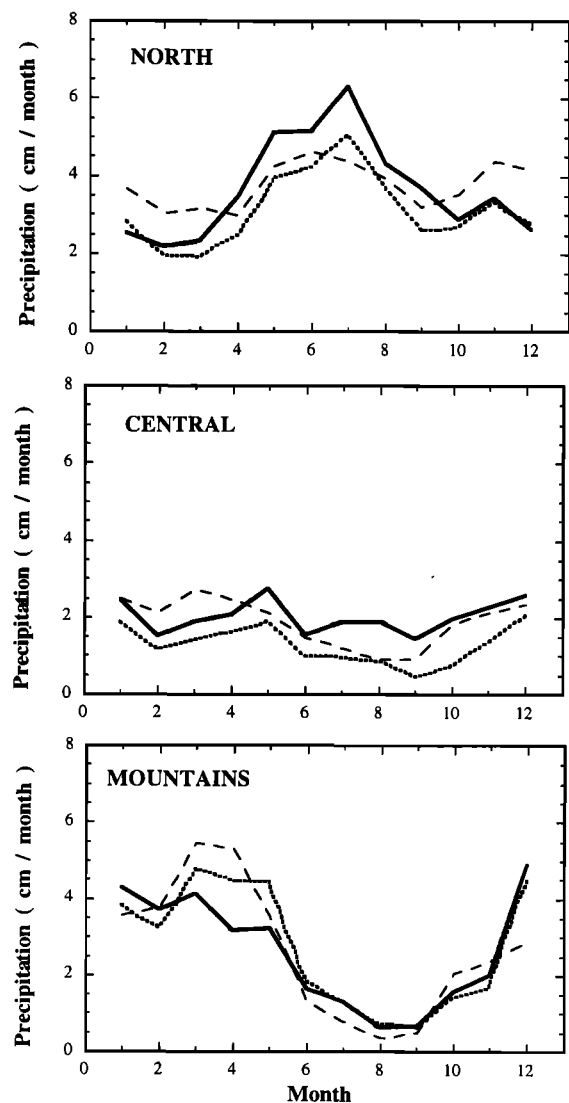

Figure 7. Monthly averaged RegCM2 precipitation (solid), CAC precipitation (dotted), and LWC corrected precipitation (dashed). Top is north, middle is central, and bottom is mountain subregion.

Table 2. Simulated and Observed Precipitation Averaged by Season and Subregion

	DJF	MAM	JJA	SON	Annual
North· Number of Stations= 12					
Model: all points	2.51	3 38	5.01	3.51	3.60
Model: cells with obs only	2.42	3.61	5.14	3.32	3.62
Observations (corrected)	2.43 (4.24)	2.65 (3.70)	4.12 (4.68)	2.75 (3.84)	2.99 (4.12)
Percent difference (corrected)	0 (-75)	26 (-3)	20 (9)	17 (-16)	17 (-14)
Central: Number of Stations= 13					
Model: all points	2.20	2.25	1.89	1.88	2.05
Model: cells with obs only	2.18	2 23	1.76	1.88	2.01
Observations (corrected)	1.70 (2.69)	1.63 (2.25)	0.92 (1.11)	0.86 (1.27)	1.28 (1.83)
Percent difference (corrected)	22 (-23)	27 (-1)	48 (37)	54 (33)	36 (9)
Mountains: Number of Stations= 22					
Model: all points	4.54	3.68	1.10	1.29	2.65
Model: cells with obs only	4.28	3 51	1.20	1 41	2 60
Observations (corrected)	3.86 (4.33)	4.55 (5.00)	1.29 (1.35)	1.25 (1.40)	2.72 (3.01)
Percent difference (corrected)	10 (-1)	-30 (-43)	-8 (-13)	11 (1)	-5 (-16)

Observed (CAC) values which include the Legates and Willmott correction are in parentheses. Units are cm/month. Percent difference calculated as (model-obs)/model.

the LWC annual cycle is noticeably less. Therefore RegCM2 and the LWC also compare favorably.

Although the model simulates the shape of the annual cycle well in each subregion, simulated precipitation values are greater than those found in the CAC data set (Figure 7). Before we can fairly compare the simulated magnitude of precipitation to observations, we must first correct the CAC data for biases resulting from the undercatch of rain gauges. We use the spatially varying, monthly precipitation correction from the LWC as an estimate of these errors. These corrections are best viewed as an estimation of the uncertainty in the precipitation data. Actual precipitation amounts likely fall between the observed and the observed plus corrected values.

When averaged seasonally, the simulated precipitation is within ±10% of the range bounded by the observed and the observed plus corrected values, except for three combinations of subregion and season. Simulated precipitation is too low during the spring over the mountains and too high during summer and fall over the central subregion (Table 2). The negative bias over the mountains during spring is probably

related to the mean circulation errors discussed above. The model's 500 mbar height bias leads to a reduced northward water vapor flux throughout the central portion of the domain (Figure 5b). During spring, northward transport of water vapor is an important source for precipitation over the mountains, and RegCM2 underestimates this source, leading to reduced precipitation.

A possible explanation for the positive precipitation bias during summer and fall over the central subregion is that the moist physics scheme is not versatile enough to reproduce the very low precipitation rates (~ 1 cm/month) observed during these seasons. The evaporation of falling precipitation is not represented by the nonconvective moist physics scheme used in this version of RegCM2. Inclusion of this process may be essential for the model to simulate accurately the limited precipitation over central Asia during summer and fall. Alternatively, the overprediction of precipitation could be related to the convection or land surface schemes, as these model components also strongly influence the summer and fall precipitation.
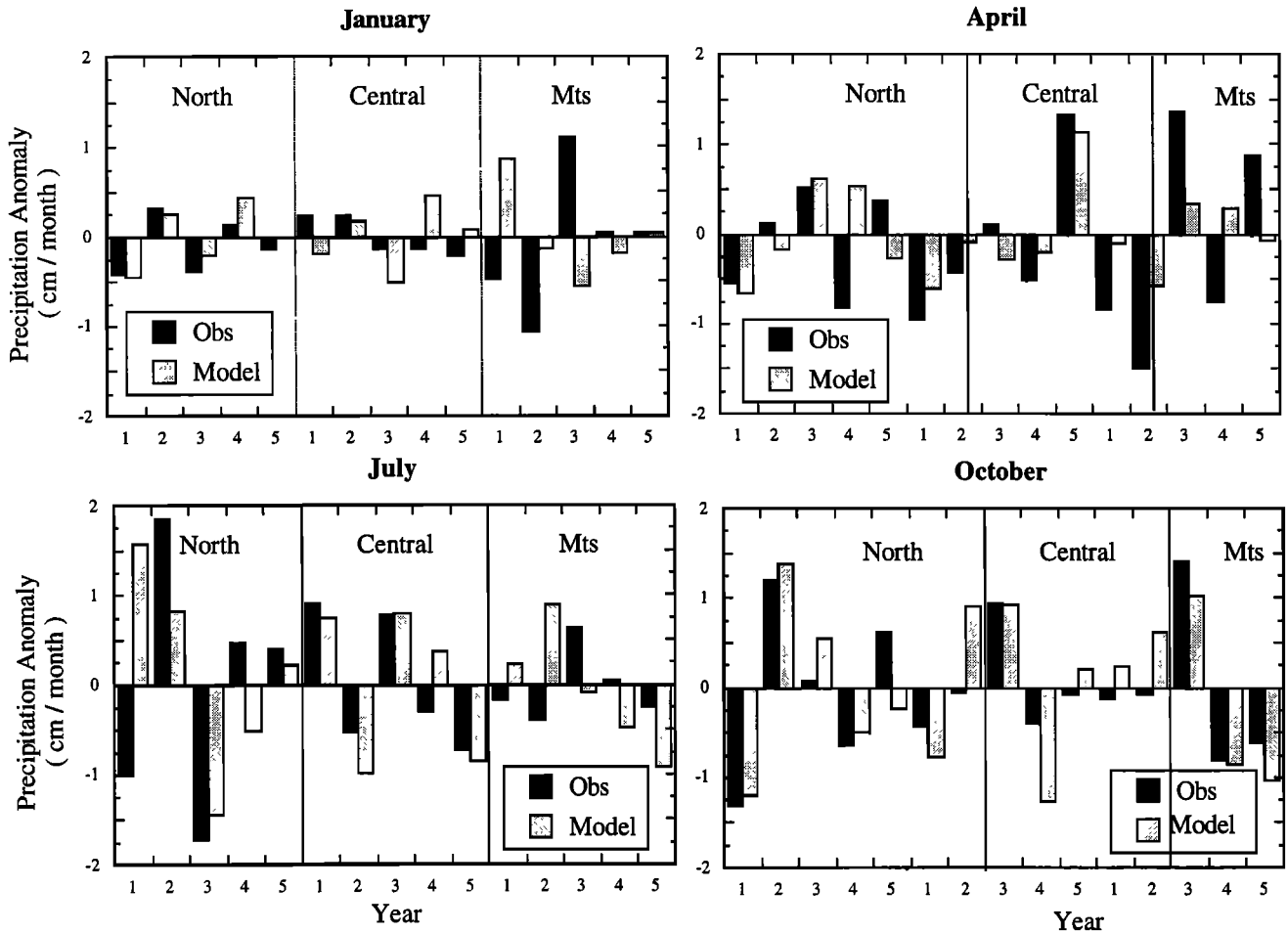
Figure 8. Five year series of paired observed (black) and simulated (gray) monthly precipitation anomalies, grouped by subregion and month. Year 1 is 1988, year 2 is 1989, etc.

5. Interannual Variability of Precipitation

In this section, we evaluate RegCM2's ability to simulate the interannual variability of precipitation observed between 1988 and 1992. We compare simulated and observed precipitation anomalies averaged by subregion because our goal is to assess how well the model simulates anomalies on a length scale of $\sim10^3$ km. We calculate simulated (RCM') and observed (OBS') monthly precipitation anomalies as follows:

$$RCM'_i{}^{s,m} = RCM_i{}^{s,m} - \frac{1}{n}\sum_{i=1}^{n} RCM^{s,m} \qquad (1a)$$

$$OBS'_i{}^{s,m} = OBS_i{}^{s,m} - \frac{1}{n}\sum_{i=1}^{n} OBS^{s,m} \qquad (1b)$$

The superscripts s and m refer to particular subregions and months; the subscript i refers to the year for which the anomaly is being calculated, and n is the number of years. The first term on the right-hand side represents the amount of precipitation for a month in a particular year (e.g., April 1989), and the second term represents the corresponding monthly mean precipitation averaged over all years (e.g., mean April precipitation). As with our analysis of mean

precipitation, these calculations only include model grid cells in which CAC meteorological stations with acceptable precipitation records are located. Corrections for the undercatch of rain gauges are not included. When calculated according to equation (1), simulated and observed anomalies may be identical for any or all months even if a bias exists between simulated and observed mean precipitation. This is important because it decouples our assessments of the model's ability to simulate the mean and the variability.

Figure 8 shows a 5-year-long series of simulated and observed precipitation anomalies for each midseason month. The simulated anomalies closely match the observed anomalies for some combinations of subregion and month. For example, the sign of the modeled anomalies is the same as observed in all five Januarys in the northern subregion. In addition, each simulated anomaly is of similar magnitude to the corresponding observed value, except in the fourth year. It is also common for there to be little similarity between the simulated and the observed anomalies. This is the case in the mountain subregion during January, for example.

We group monthly anomalies by season prior to computing statistics that summarize the relationship between simulated and observed anomalies. This results in 15 pairs of simulated and observed anomalies for each season in each subregion, increasing the sample size over which statistics are calculated.

Of course, the 15 paired anomalies are not fully independent because some autocorrelation between monthly anomalies from the same year should exist. This issue is addressed further below.

After grouping the subregion-averaged monthly precipitation anomalies by season, we compare each set of simulated and observed anomalies in two ways. First, we compare simulated and observed standard deviations, which is a measure of the magnitude of year-to-year changes relative to the mean. Second, we calculate a correlation coefficient r for each set of simulated and observed anomaly pairs. The correlation coefficient indicates the degree to which there is a linear relationship between the simulated and the observed values. When r is zero, there is no relationship between the simulated and the observed anomalies. When r is 1, a perfect, positive, linear correlation exists. However, this does not indicate there is a 1:1 correspondence between simulated and observed anomalies. For our use, r measures whether or not months that are wetter than average in the observations are also wetter than average in the model, and vice versa. In addition, r indicates if the scaling between simulated and observed anomalies is constant.

5.1. Scale of Variability

Overall, the scale of variability simulated by the model is similar to that found in the CAC data set. During summer, simulated and observed standard deviations are nearly equal in the north and central subregions (Figure 9, Table 3). In the mountains the simulated value is somewhat less than the observed value. As shown above, RegCM2 reproduces the high meridional mean precipitation gradient during this season (Figure 6). The model also reproduces the large summertime difference in variability between the northern subregion and the rest of the domain, 1.20 cm compared to 0.62 cm (Figure 9, Table 3). A similar relationship between simulated and observed variability exists during spring. Whereas simulated and observed standard deviations nearly match in the north and central subregions, the simulated value is much less than the observed value in the mountains (Figure 9, Table 3). During fall the scale of variability is simulated well except in the central subregion, where the simulated variability is too high. The greatest domain-wide difference between simulated and observed magnitudes of variability exists during winter. In this season the simulated standard deviation is noticeably greater than observed in all three subregions: the ratio of simulated to observed values is >= 1.3. Although the simulated and observed magnitudes differ during winter, the model does reproduce the observed pattern of variability, being higher in the mountains than in the rest of the domain. On the basis of an F-test (α = 0.05) the simulated and observed variabilities are different only for the central region during the fall and winter. If the sample size is reduced to account for autocorrelation, the differences in these cases would no longer be significant. Obviously, a longer simulation would be more useful for drawing statistical inferences.

Before comparing the magnitude of simulated and observed mean precipitation, we corrected the observations for the undercatch of rain gauges. To estimate the effect of undercatch on the comparison of anomalies, we calculated corrections for individual monthly anomalies in the following way. Consider a rain gauge that catches a constant fraction of the total
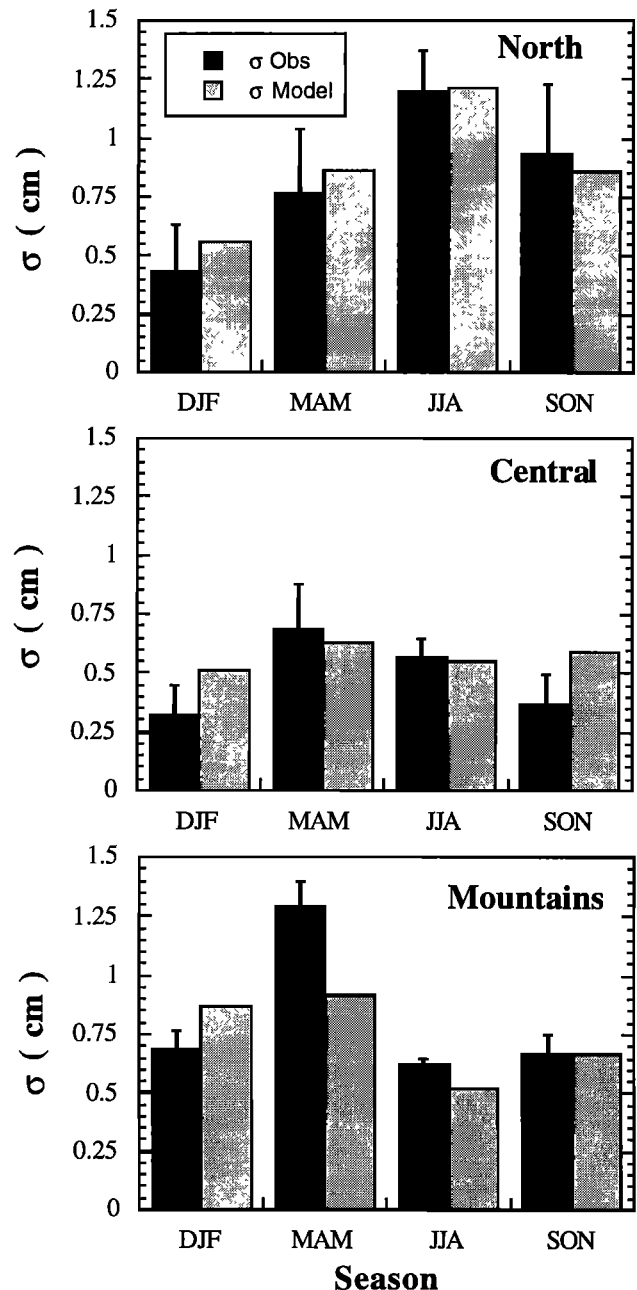

Figure 9. Standard deviation (σ, in cm) of interannual variability of precipitation by season: observed (black) and simulated (gray). The error bars show the observed variability when undercatch of rain gauges is included. Top is north, middle is central, and bottom is mountain subregion.

precipitation. For a month drier than the mean, the correction should be less than the mean correction, or the value used to adjust the observations in the LWC. Likewise, the correction for a wet month should be greater than the mean correction. In the case of a constant fraction of undercatch, the correction for a particular month $C_i^{s,m}$ is

$$C_i^{s,m} = \frac{(OBS_i^{s,m})}{(<OBS^{s,m}>)} <C^{s,m}>$$

(2)

where $OBS_i^{s,m}$ is the monthly precipitation total, $\langle OBS^{s,m}\rangle$ is the mean precipitation for that month, and $\langle C^{s,m}\rangle$ is the

Table 3. Comparison of Simulated and Observed Precipitation Variability

	DJF	MAM	JJA	SON
	$\sigma_{RCM} / \sigma_{OBS} = Ratio$			
North	0.56 / 0.43 = 1.30	0.86 / 0.77 = 1.12	1.21 / 1.20 = 1.01	0.86 / 0.93 = 0.92
Central	0.51 / 0.32 = 1.59	0.63 / 0.69 = 0.91	0.55 / 0.57 = 0.96	0.59 / 0.37 = 1.59
Mountains	0.87 / 0.69 = 1.26	0.92 / 1.29 = 0.71	0.52 / 0.62 = 0.84	0.67 / 0.67 = 1.00
	$\sigma_{RCM} / \sigma_{OBS}$ (corrected)			
North	0.89	0.83	0.88	0.70
Central	1.15	0.72	0.85	1.20
Mountains	1.14	0.66	0.80	0.89
	Correlation Coefficient r			
North	0.84	0.74	0.19	0.77
Central	0.59	0.55	0.65	0.67
Mountains	0.00	0.72	0 00	0.51

(top) Simulated (RCM) and observed (OBS) standard deviation (s) in cm and resulting ratio (middle) Ratio of simulated and observed plus corrected standard deviations (bottom) Correlation coefficient r for simulated and observed anomaly pairs

mean monthly correction. The superscripts and subscripts are the same as in equation (1).

The magnitude of observed variability is substantially higher when this linearly scaled correction is added to the observed anomalies (Figure 9). This decreases the ratio of simulated to observed variability (Table 3). Changes are particularly large during the winter, when high winds and snow result in the greatest LWC mean corrections (Table 2). Thus a possible explanation for the discrepancy between the magnitude of simulated and observed wintertime variability is that the observed variability is underestimated because of the undercatch of rain gauges. We do not suggest that a linearly scaled correction accurately depicts conditions in central Asia. Instead, our approximation is intended to show that the magnitude of variability calculated from uncorrected observations may underestimate the true variability. This issue should be addressed in future research.

5.2. Comparison of Anomaly Pairs

Whereas RegCM2 closely reproduces observed anomalies in many combinations of season and subregion, there is little or no relationship between simulated and observed anomalies in others. During winter, each simulated anomaly is nearly the same as the corresponding observed anomaly in the north subregion (Figure 10a). Particular months that are wetter (drier) than average in the observations are wetter (drier) than average in the simulation. The correlation coefficient r for the paired anomalies during winter is 0.84, which indicates a strong positive, linear relationship between the simulated and

the observed anomalies (Table 3). For 15 independent samples, r values exceeding 0.4 indicate a positive, linear correlation at the 95% confidence level. In the central region the similarity between wintertime anomaly pairs is not so high as in the north, but the r value (0.59) suggests that a positive, linear correlation still exists. In the mountains, there appears to be no relationship between the simulated and observed wintertime anomalies (Figure 10a). Regardless of whether or not the 15 anomaly pairs represent fully independent samples, the wintertime result is clear; there is a strong north-south gradient in how closely RegCM2 reproduces the observed anomalies.

During spring and fall, simulated and observed anomalies are positively correlated in each subregion (Figures 10b and 10d). This correlation is strongest in the north subregion. During fall, there is a north-south gradient in the RegCM2 reproduction of anomalies, which is similar to the wintertime result. Although the correlation between anomaly pairs is high during these two seasons (r > 0.4), the magnitudes of simulated and observed variability do not necessarily compare well ($\sigma_{RCM} / \sigma_{OBS} \neq 1$) (Table 3). Relative to the observations, the simulated scale of variability (σ) is lower in the mountains during the spring and higher in the central region during the fall than in any other combination of season and region. During summer the correlation between simulated and observed anomalies is weak or nonexistent in the north and mountains subregion and moderate in the central subregion (Figure 10c). The magnitude of variability is simulated well even though the correlation between anomaly
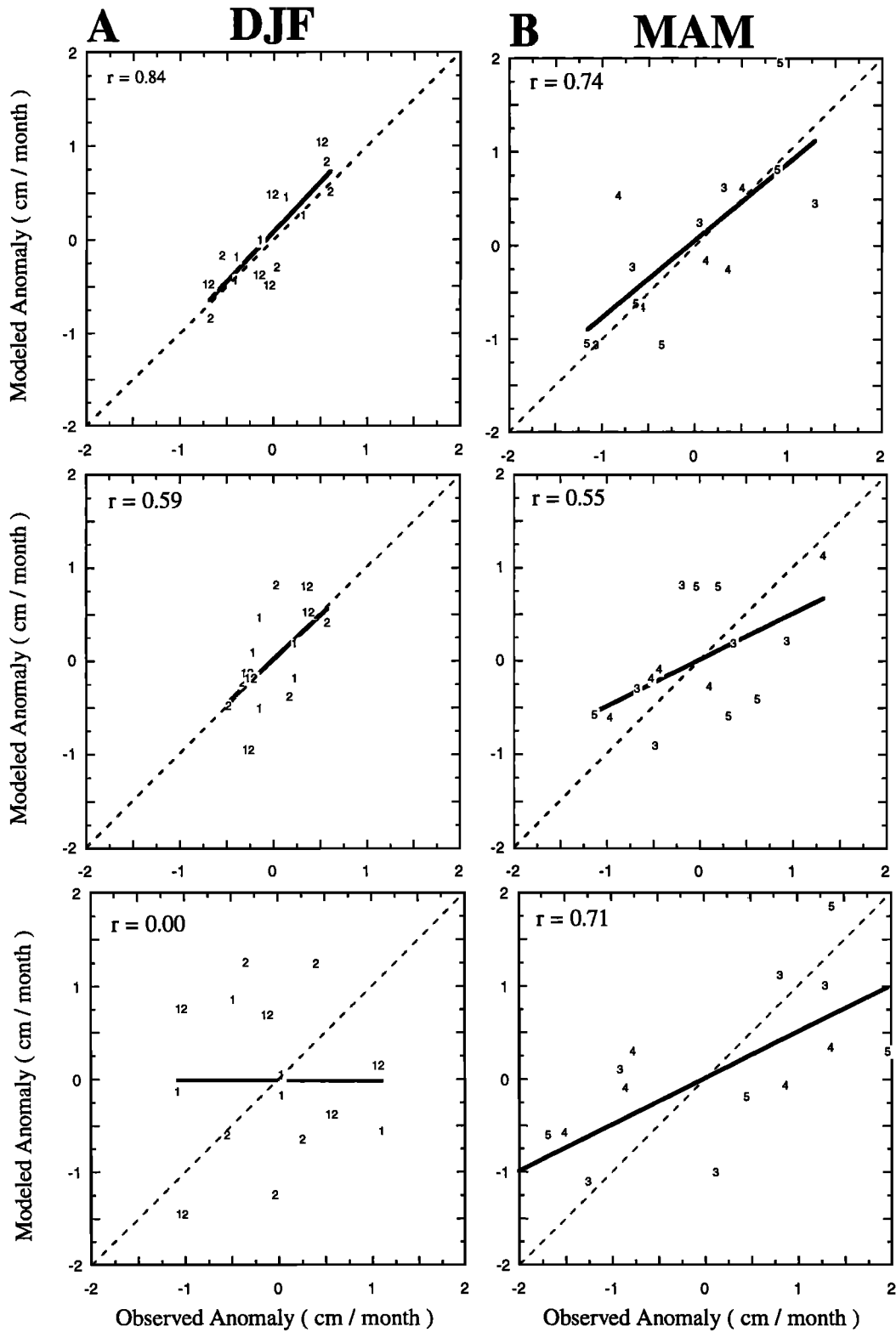
Figure 10. Simulated versus observed monthly precipitation anomalies, grouped by season and subregion: (a) winter, DJF; (b) spring, MAM; (c) summer, JJA; and (d) fall, SON. Top is north, middle is central, and bottom is mountain subregion. Numbers indicate month of particular simulated-observed anomaly pair. Dashed line is 1:1 line. Solid line is least squares linear fit. Correlation coefficient r is shown for each plot.
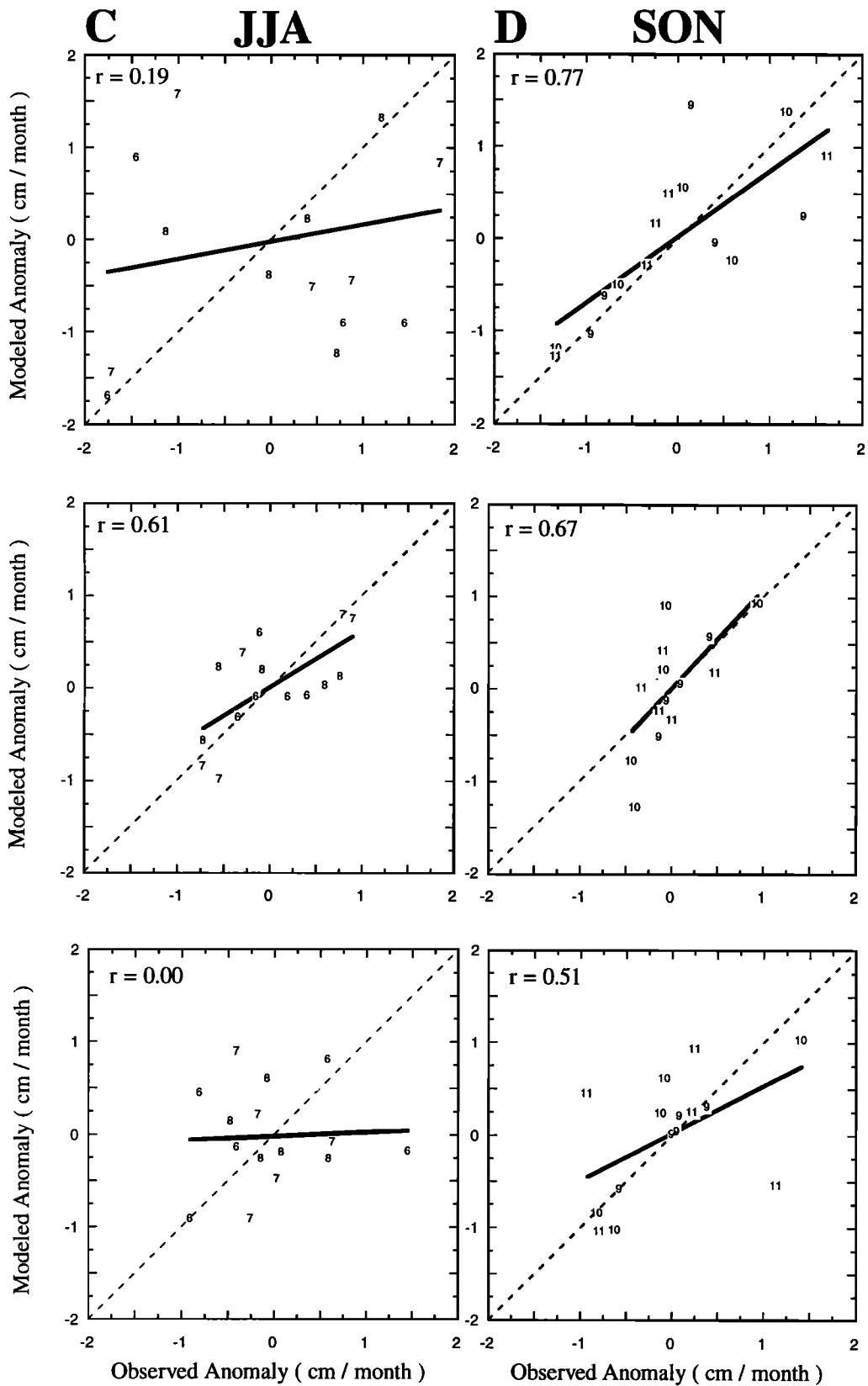
Figure 10. (continued)

pairs is weak (Table 3). This is the opposite of what was found during spring and fall. On the basis of these results for spring through fall, it appears as if the model's abilities in simulating the magnitude of variability and in reproducing particular anomalies are not strongly linked.

6. Discussion

A high correlation between a series of simulated and observed anomalies is an indication of strong model performance. In particular, this shows that (1) the boundary condition assimilation transmits the year-to-year changes in synoptic scale conditions into the domain; (2) the model successfully simulates the dynamic evolution of circulations within the domain and their effect on precipitation; and (3) year-to-year changes in land surface characteristics (e.g., soil moisture or snow cover) and the associated variations in land-atmosphere interactions are successfully simulated.

If month-long precipitation anomalies are consistently reproduced by RegCM2, then the anomalies over some region must be controlled by the two climate features which vary from year-to-year in the model. These are (1) the synoptic scale atmospheric conditions which are applied at the domain boundaries; and (2) the characteristics of the land surface, including soil moisture, snow cover, and surface temperature, which influence land-atmosphere interactions. Precipitation anomalies must also be controlled by the weather that has affected the domain during the preceding months, because the condition of the land surface is partially set by previous weather conditions. Randomness within the model domain must have a lesser influence on precipitation anomalies than the atmospheric conditions at the domain boundaries and the conditions of the land surface. The implication for predicting climate anomalies is as follows: If an ensemble of coupled ocean-atmosphere GCM (AOGCM) integrations can provide an accurate description of the evolution of synoptic scale atmospheric conditions from some initial state, then regional scale precipitation anomalies can be accurately reproduced with a single nested model simulation for each AOGCM run. This eliminates the need to complete a series of nested model integrations for each member of an AOGCM ensemble. The results described above show that month-long precipitation anomalies in central Asia are predictable without a nested model ensemble approach, given accurate boundary conditions. The exceptions to this are the summer months and the mountains during winter.

When the model fails to reproduce a series of anomalies, as is the case during the summer, one or several factors may be responsible. One possibility is that the year-to-year changes in synoptic scale circulations, temperature, and specific humidity are not adequately represented in the ECMWF analyses. There is no way for RegCM2 to reproduce a series of observed anomalies if the large scale forcing of variability is not included in the boundary conditions, unless the variability is entirely due to deterministic processes within the domain. It is conceivable that the ECMWF analyses are imperfect in data-sparse regions like central Asia; however, we do not evaluate this issue further in this paper. More likely, the model's failure to reproduce anomalies during summer and in the mountains during winter is due to internal model errors and/or lower predictability of anomalies. We examine these two factors in the following sections.

6.1. Relationship Between Circulations and Anomalies

If RegCM2 does not reproduce the atmospheric conditions that prevailed during a particular month (e.g., April 1989), then it is unlikely that the model will successfully simulate the corresponding observed precipitation anomaly. This may be the reason why RegCM2 does not reproduce anomalies in the summer and in the mountains during winter. Above we showed that the model simulates the mean circulations well; however, this is not proof that the model closely replicates the atmospheric state in a particular month. To assess how closely RegCM2 reproduces actual anomalous circulations, we compare RegCM2 and ECMWF 500 mbar geopotential height fields at 12-hour intervals. This is not a true comparison between simulated and actual circulations; however, the ECMWF fields represent our best guess of the atmospheric fields that actually existed. We calculate a 500 mbar height variance reduction (VR) field for each month, from the series of five realizations of that month (1988-1992).

$$VR = 1 - (\sum_{i=1}^{n}(RCM'_i - OBS'_i)^2/\sigma^2_{OBS} \qquad (3)$$

The model (RCM') or ECMWF (OBS') 500 mbar height anomaly at some time is equal to the height at that time minus the monthly mean value from the five simulated years. Variance reduction is a useful statistic to assess time-dependent circulation differences because the squared error between model and ECMWF anomalies is normalized by the observed variance (σ^2_{OBS}). This normalization allows for comparison between months with different amounts of 500 mbar height variability. For our application, the value of variance reduction can be thought of as the fraction of observed (ECMWF) variability reproduced by RegCM2. When VR is equal to 1, model and ECMWF 500 mbar height anomalies are identical at all times. Lower values of VR indicate greater time-dependent differences between the model and the ECMWF.

The pattern of 500 mbar height variance reduction is similar for each midseason month (Figure 11). The value of VR is equal to 1 at the domain edges where the model solution is forced to match ECMWF. Values decrease toward the interior of the domain because RegCM2 circulations evolve without boundary condition constraints away from the domain edges. Overall, values of variance reduction are lowest during July and highest during January and April. In each month, the pattern of decreasing VR toward the interior of the domain is not symmetric. For example, the lowest variance reduction values are closer to the eastern and southern boundaries of the domain during January (Figure 11). These asymmetries in the variance reduction pattern are spatially related to the mean atmospheric flow fields. VR is relatively high at locations of strong inflow and relatively low near the outflow boundaries. For example, the high VR in the southwest corner of the domain during April is located in an area with strong inflow (Figure 5). We have also calculated VR fields for sea level pressure and vertically integrated water vapor flux, with similar results.

The seasonal and spatial variability in RegCM2-ECMWF circulation differences (shown in the VR maps) is largely controlled by variations in the time that individual circulation systems persist within the domain. Differences between
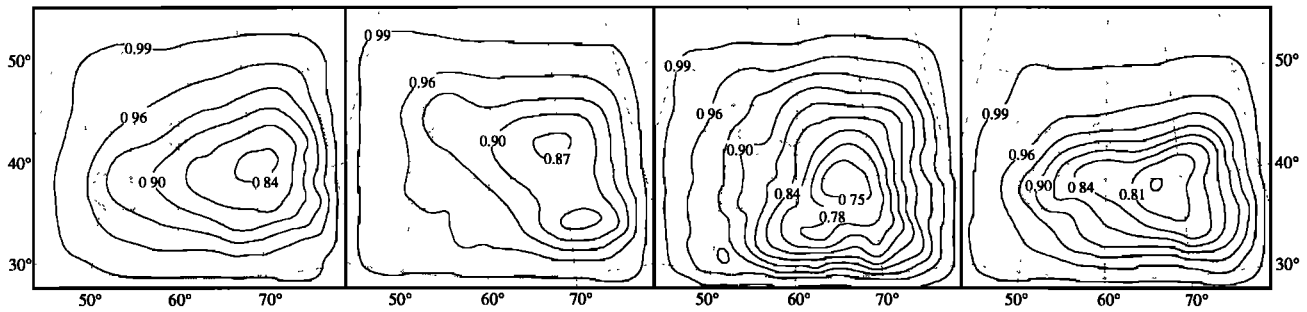
Figure 11. Maps of 500 mbar geopotential height variance reduction for January, April, July, and October (left to right). Contour interval is 0.03, starting at 0.99.

simulated and observed circulations grow with increasing residence time, as dynamical instabilities and nonlinear interactions amplify differences introduced by imperfect boundary conditions and model approximations and errors [*Shukla*, 1981]. Typical domain residence times are greatest during summer because the zonal circulations are weakest at this time of year (Figure 4). Accordingly, the VR fields show that simulated and observed (ECMWF) circulations are most different during this season (Figure 11). RegCM2's failure to reproduce precipitation anomalies during summer is at least partially due to the relatively large differences between simulated and observed atmospheric conditions at this time of year. This same relationship was found by *Luthi et al.* [1996] for a domain covering Europe.

Within a particular season, the residence time of circulation systems increases along atmospheric flow paths, so it makes sense that simulated and observed circulations are relatively similar in the vicinity of strong inflow and relatively different near outflow boundaries. This relationship may explain the high interregion variability in the reproduction of precipitation anomalies during winter (Figure 10a). During winter, circulations move progressively from the north to the central and finally to the mountains subregion. Along this path, the correlation between simulated and observed precipitation anomalies decreases as RegCM2-ECMWF circulation differences grow. The January 500 mbar height variance reduction minimum is centered at ~70°E 40°N, directly over most of the stations in the mountain subregion (Figure 1). In this region, there is no relationship between the simulated and the observed precipitation anomalies. During spring through fall, circulations travel across each subregion from west to east because flow is more zonal (Figure 4). Therefore the residence time of circulations is similar in each subregion, and the subregion differences in precipitation anomaly correlations are not so dramatic.

The magnitude of simulated and observed circulation differences probably strongly influences the reproduction of precipitation anomalies; however, these differences do not fully explain the spatial and seasonal variations in RegCM2's ability to reproduce anomalies. For example, the difference between simulated and observed circulations is slightly greater in the central region during spring (VR = ~0.90) than in the north subregion during summer (VR = ~0.95). However, the correlation between simulated and observed precipitation anomalies is greater in the central region (r = 0.55) than in the north (r = 0.19) (Table 3). In the next section, we examine how precipitation patterns influence the predictability of

anomalies and show that they probably affect RegCM2's simulation of interannual variability in central Asia.

6.2. Influence of Precipitation Patterns on Simulation of Anomalies

To understand more fully what the spatial and seasonal variability in simulated-observed precipitation anomaly correlations (Figure 10) indicates about model performance and the predictability of climate anomalies in central Asia, it would be useful to answer the following question: In two different locations or seasons, do identical modeled-observed differences in atmospheric conditions lead to equal precipitation anomaly errors? In other words, does the sensitivity to circulation "errors" vary seasonally and spatially? Unfortunately, we cannot directly address this question because we have only one model representation of the simulated atmospheric circulations and associated precipitation anomaly error for each observed monthly precipitation pattern. Because of this shortcoming, we are forced to address a slightly different question. In two different locations or seasons, do identical simulated-observed differences in precipitation patterns lead to equal precipitation anomaly errors? Because precipitation patterns are tightly linked to atmospheric circulations in many situations, we assume that shifted precipitation patterns are a suitable proxy for displaced atmospheric circulations.

To address the latter question, we analyze a data set generated by translating observed precipitation patterns and calculating the resulting precipitation anomaly error. We intend for the translated precipitation patterns to represent the simulated precipitation that would arise when the model displaces atmospheric circulations, e.g., when a simulated storm trajectory is offset from the observed path. Equating translated precipitation patterns with translated atmospheric circulations simplifies reality in that modeled precipitation will not shift uniformly with displaced circulations, largely because of surface forcing from topography and soil moisture. In addition, our approach only includes the uniform translation of patterns, whereas simulated-observed circulation differences are more complicated. We substitute "translated circulations" for "translated precipitation patterns" in the following discussion, as we are assuming they are interchangeable.

Our synthetic data set is generated according to the following steps: First, we interpolate the observed precipitation for some month (e.g., January 1988) onto the
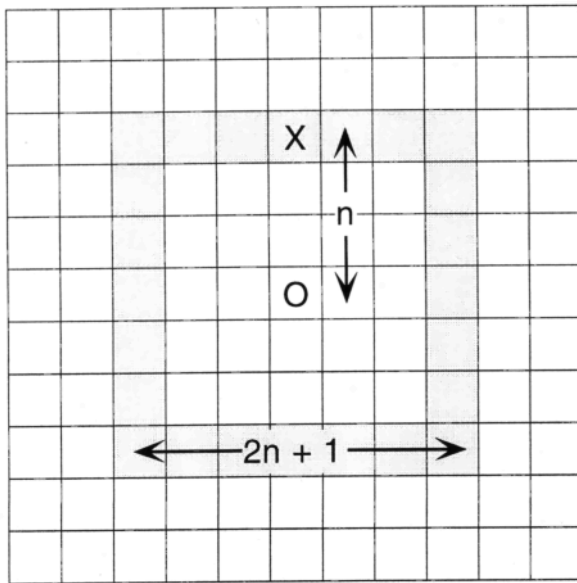
Figure 12. A series of synthetic simulated-observed anomaly pairs is generated by repeatedly translating the observed precipitation pattern a set distance n in the N-S or E-W direction. Relative to the origin O the pattern is shifted to all points (x, for example) on a square which is $2n$ on a side (shaded) . This results in $8n$ synthetic pairs for each translation distance.

model grid. Second, the observed precipitation field is translated a specified distance or number of grid cells from the origin n in either the N-S or the E-W direction (Figure 12). Third, anomalies are calculated from the translated and original precipitation patterns for each subregion according to equation (1). This results in one synthetic pair of "simulated" (from the translated observations) and observed precipitation anomalies. Fourth, the translation of distance n and subsequent anomaly calculation is repeated (8n times) until the observed pattern has been moved to every point at the specified distance (n) from the origin (Figure 12). Fifth, for the same translation distance (n), the above steps are repeated with the observed precipitation pattern from the same month (January) in subsequent years (1989-1992). Finally, a correlation coefficient is calculated from the series of synthetic and observed anomalies. This correlation coefficient describes the correspondence between the observed anomalies and the anomalies which result from a uniform translation in a certain month (January). The process is repeated for different translation distances, varying from 1 to eight grid cells or 50 - 400 km, as well as for all 12 months.

Figure 13 shows how the correlation coefficient between our synthetic and observed anomaly pairs r_{syn} varies with translation distance for each subregion in January and July. In all cases the correlation between anomalies decreases as the observed precipitation pattern is translated a greater distance. However, the rate at which r_{syn} declines is not uniform (Figure 13). For example, a translation of 250 km over the north subregion produces very different r_{syn} values in January and July, ~0.8 and ~0.5, respectively. This suggests the following answer to the question posed above. In two different months or locations, identical simulated-observed circulation differences may produce unequal precipitation
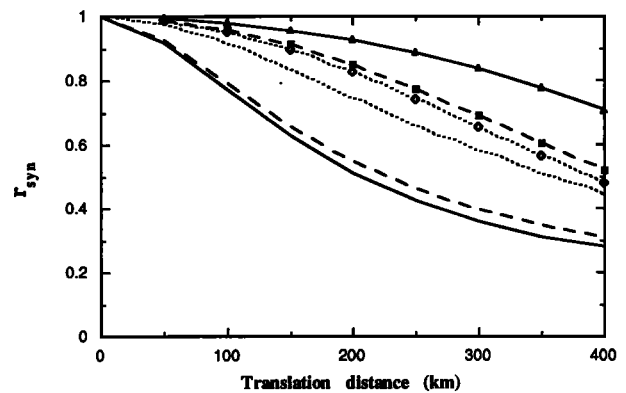

Figure 13. The synthetic correlation coefficient r_{syn} versus translation difference for the north (dashed), central (dotted), and mountain (solid) subregions. Lines with points represent January, lines without points represent July.

anomaly errors, assuming that precipitation anomalies are closely linked to atmospheric circulations. This result is also apparent in the annual cycle of r_{syn} for each subregion for a constant translation distance of 250 km (Figure 14). In the north and mountain subregions, the errors in precipitation anomalies resulting from a 250 km translation are much greater during the summer than in other seasons. The pattern is slightly different in the central subregion, where maximum errors exist during May and June. In December through June, precipitation anomalies over the mountain subregion are the least sensitive to shifted patterns. Individual monthly values of r_{syn} are higher or lower for other translation differences; however, the shape of the annual cycle remains nearly the same.

Monthly variations in the value of r_{syn} for a certain translation distance (Figure 14) reflect changes in spatial precipitation gradients across the different subregions. Relatively large (small) anomaly errors occur when patterns are shifted across areas with high (low) precipitation gradients. For example, pattern translation across the strong meridional precipitation gradient which exists over the north subregion during summer (Figure 6) results in relatively large anomaly errors (Figure 14).
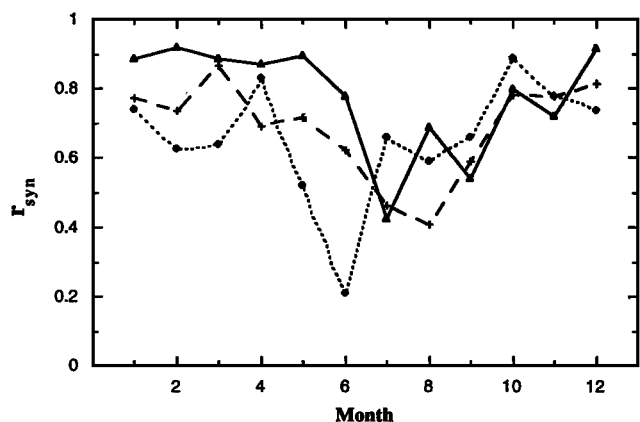

Figure 14. Seasonal cycle of r_{syn} for each subregion, for a constant translation of 250 km. North is dashed, central is dotted, and the mountains subregion is solid.

In the simulation examined here, modeled and observed monthly precipitation fields often exhibit similar patterns and magnitudes. However, the simulated patterns are frequently shifted several hundred kilometers in one or another direction relative to the observations. In many of these cases the corresponding simulated and observed precipitation anomalies differ greatly in magnitude and sign (Figure 8). Therefore the results gleaned from our comparison of synthetic anomaly pairs may be useful to understand the simulation examined here. The relationship between the strength of precipitation gradients and the magnitude of anomaly errors is probably most important during spring and summer. To a first approximation the location of the highest precipitation gradient is controlled by the position of the jet stream during these seasons. If RegCM2 misplaces the position of the jet stream and the associated storms and precipitation by several grid cells (~200 km), the simulated precipitation anomalies in the north and central subregion will differ greatly from observed (Figures 13 and 14). The pattern translation results are not so useful to understand model performance in the mountains, because orographic forcing limits the degree to which simulated precipitation will simply shift with misplaced atmospheric circulations.

6.4. Summary of Model Performance in Reproducing Anomalies

The failure of RegCM2 to reproduce precipitation anomalies during summer is not necessarily a mark of poor model performance. Instead, it suggests that precipitation anomalies are less predictable during this season because of several different factors. First, the reproduction of actual circulation systems, and therefore the simulation of precipitation anomalies, is relatively difficult during summer. Flow through the model domain is weakest during this season, increasing the time during which simulated and observed differences in atmospheric conditions can grow. These differences are expected in models of the atmospheric system, with or without model errors. Second, as spatial precipitation gradients are highest during summer, simulated-observed circulation differences produce the largest anomaly errors during this season. These two influences operate together during summer, limiting the likelihood that RegCM2 can reproduce the precipitation anomalies associated with certain synoptic scale atmospheric conditions. Third, summer convective processes are inherently more random than the precipitation mechanisms that dominate in other seasons, which also decreases the predictability of summertime anomalies [Luthi et al., 1996]. Even though the model fails to reproduce particular summertime anomalies, it does simulate the magnitude of variability well in each subregion. This may be a more important model diagnostic during seasons in which precipitation anomalies are relatively difficult to reproduce.

The model's failure to reproduce wintertime anomalies in the mountains may denote inadequate model performance, because these anomalies should be relatively easy to predict, at least in terms of the sensitivity to displaced atmospheric circulations (Figure 14). In addition, simulated-observed differences in atmospheric conditions are not large, especially when compared to other situations in which precipitation anomalies are simulated more closely (e.g., during fall in the mountains). The source of model errors during winter over the mountains is not obvious. The relatively smooth model topography or low station density in the mountains may contribute to the problem.

7. Comparison of Simulated Mean and Variability

In this section, we compare how well RegCM2 simulates the mean and variability of precipitation in particular seasons and subregions. Excluding the winter season, there appears to be a positive correlation between the model's biases in simulating (1) mean precipitation and (2) the magnitude of precipitation variability. RegCM2 tends to underpredict (overpredict) the magnitude of variability in the same combinations of subregion and season for which it underpredicts (overpredicts) mean precipitation (Figure 15). In addition, the magnitude of the variability tends to be simulated well when mean precipitation closely matches observed values. For example, the most severe underestimates of both mean precipitation (Table 2) and the magnitude of interannual precipitation variability (Table 3) occur in the mountains during spring and summer. The most serious overestimates of both mean precipitation and variability exist in the central region during fall. An exception to this relationship is the central region during summer, when mean precipitation is clearly overestimated but the ratio of simulated to observed variability is close to 1. During winter the positive correlation between mean and variability model biases does not hold. This could be related to the large uncertainty in wintertime observations due to snow and high wind speeds, depicted by the error bars in Figure 15.

Unlike the positive correlation between biases in the mean and the magnitude of variability, there appears to be no
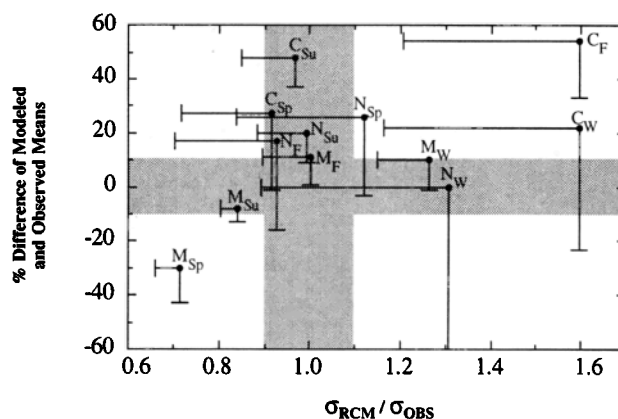

Figure 15. Percent difference between simulated and observed mean precipitation (y axis) versus the ratio of the simulated and observed standard deviation ($\sigma_{RCM}/\sigma_{OBS}$) of precipitation (x axis). There is one point for each combination of season and subregion. N is north, C is central, and M is mountains. The subscripts denote season: W is winter, Sp is spring, Su is summer, and F is fall. Bars in the y direction show the range spanning from the percent difference between simulated and observed means (end with the circle) and the percent difference between simulated and observed plus corrected means (see Table 2). Bars in the x direction span from the ratio of the simulated and observed standard deviations (σ) to the ratio of the simulated to observed plus corrected standard deviations (σ) (see Table 3). The shaded areas represents ±10% of the mean and ratios between 0.9 and 1.1.
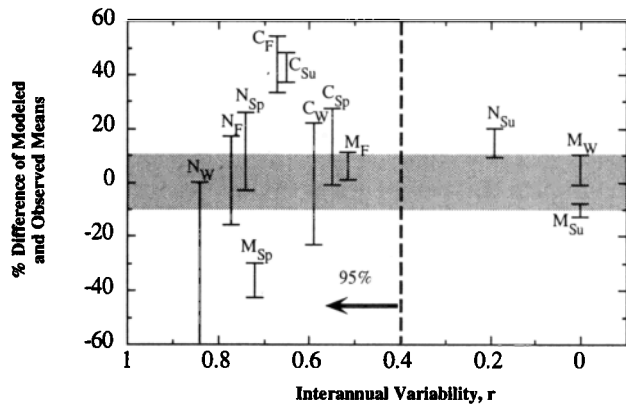
Figure 16. Same as Figure 14, but the correlation coefficient describing how closely RegCM2 reproduces a series of precipitation anomalies is plotted on the x axis. The dashed line indicates the minimum r value for which a positive linear correlation is significant at the 95% confidence level.

connection between model biases in mean precipitation and the model's skill in reproducing a series of precipitation anomalies (Figure 16). In nine of the twelve combinations of season and subregion, RegCM2 simulates the mean precipitation well. In these situations the simulated precipitation is within ±10% of the range defined by the uncertainty in the observed values. The mean is not simulated well in the central subregion in the summer and fall and in the mountains in the spring. Surprisingly, the year-to-year changes in precipitation are simulated relatively well (r = ~0.7) in these three cases (Figure 16). Alternatively, precipitation anomalies are reproduced consistently in nine of the twelve combinations of season and subregion. The exceptions include the mountains in the summer and winter and the north subregion in summer. In these three cases the simulated and observed anomaly pairs do not match, but mean precipitation is simulated well (Figure 16).

These results show that RegCM2's ability to simulate mean precipitation and reproduce particular precipitation anomalies is decoupled. This result has several implications concerning RCM performance. First, the simulated processes that control mean precipitation and the interannual variability of precipitation are not entirely the same. Mean precipitation is simulated poorly by RegCM2 near inflow boundaries (Figure 6). At the same time, the model reproduces well the precipitation anomalies close to inflow boundaries. This contrast may also describe the performance of other RCMs. Second, a skillful simulation of mean precipitation does not ensure that a RCM responds correctly to a variety of synoptic scale conditions. Therefore evaluating a RCM's ability to simulate both quantities is a more demanding test of model performance than only comparing simulated and observed mean precipitation. Third, it may be difficult to assess model performance from a short simulation (e.g., several months or a year long). A model that is capable of simulating mean precipitation over several years may not accurately reproduce the observed precipitation accumulating during a particular month. This has implications for tuning model parameters. On the basis of a short simulation it may appear that model parameters need to be adjusted; however, the parameters may

already be set at the optimal value to reproduce mean precipitation.

8. Conclusions

RegCM2 simulates the mean precipitation observed in central Asia well; however, some problems do exist. First, precipitation is too low in areas of strong inflow, which suggests that the cloud water mixing ratio does not increase fast enough through the buffer zone. Second, simulated precipitation is too low over the mountains in the spring. The source of this problem is an error in mean atmospheric circulations, which results in a reduced northward water vapor flux compared to the ECMWF analyses. Third, there is a positive precipitation bias during summer and fall over the central portion of the domain, which is the region with the lowest precipitation rates (~ 1 cm/month). This bias shows RegCM2 is not versatile enough to simulate the full range of precipitation observed across central Asia.

The magnitude of simulated interannual precipitation variability is similar to that found in the CAC data set. The greatest domain-wide difference between simulated and observed magnitudes of variability exists during winter, when the ratio of simulated to observed standard deviations is >= 1.3 in all subregions. Excluding the winter season, there appears to be a positive correlation between the simulated biases in (1) mean precipitation and (2) the magnitude of precipitation variability. RegCM2 tends to underpredict (overpredict) the magnitude of variability in the same combinations of subregion and season for which it underpredicts (overpredicts) mean precipitation.

In many cases, RegCM2 closely reproduces the precipitation anomalies observed in specific months which are associated with certain synoptic scale atmospheric conditions. This indicates (1) that the boundary condition assimilation is successful and that the model accurately reproduces the evolution of circulations within the domain and its effects on precipitation; and (2) month-long precipitation anomalies are controlled by the synoptic-scale atmospheric conditions and the characteristics of the land surface, as these are the climate features that change from year-to-year in the model. The failure of RegCM2 to reproduce precipitation anomalies during summer is not necessarily a mark of poor model performance, as precipitation anomalies are less predictable during this season. However, the failure to reproduce wintertime anomalies in the mountains may denote inadequate model performance, as these anomalies should be relatively easy to predict.

Unlike the positive correlation between biases in the mean and magnitude of variability, there appears to be no connection between model biases in mean precipitation and how closely the model reproduces a series of precipitation anomalies. Therefore evaluating a the ability of a RCM to simulated both mean precipitation and precipitation anomalies is a more demanding test of model performance than only comparing simulated and observed mean precipitation.

References

Anthes, R. A., E. Y. Hsie, and Y. H. Kuo, Description of the Penn State/NCAR mesoscale model version 4 (MM4), *NCAR Tech. Note, NCAR/TN-282*, 66 pp., Natl. Cent for Atmos. Res., Boulder, Colo., 1987.

Briegleb, B. P., Delta-Eddington approximation for solar radiation in the NCAR community climate model, *J. Geophys. Res., 97*, 7603-7612, 1992.

Dickinson, R. E., R. M. Errico, F. Giorgi, G. T. Bates, A regional climate model for the western United States, *Clim.. Change, 15*, 383-422, 1989.

Dickinson, R. E., A. Henderson-Sellers, and P J. Kennedy, Biosphere-atmosphere transfer scheme (BATS) version 1e as coupled to the NCAR community climate model, *NCAR Tech. Note, NCAR/TN-387+STR*, 72 pp., Natl. Cent. for Atmos. Res., Boulder, Colo., 1993.

Giorgi, F., Simulation of regional climate using a limited area model nested in a general circulation model, *J. Clim., 3* , 941-963, 1990.

Giorgi, F., Perspectives for regional earth system modeling, *Global Planet. Change, 10*, 23-43, 1995.

Giorgi, F., and G. T. Bates, The climatological skill of a regional model over complex terrain, *Mon. Weather Rev., 117*, 2325-2347, 1989.

Giorgi, F., and C. Shields, Tests of precipitation parameterizations available in the latest version of the NCAR regional climate model (RegCM) over the continental United States, *J. Geophys. Res.,* this issue.

Giorgi, F., G. T. Bates, and S. J. Nieman, The multiyear surface climatology of a regional atmospheric model over the western United States, *J. Clim., 6*, 75-95, 1993a.

Giorgi, F., M. R. Marinucci, and G. T. Bates, Development of a second-generation regional climate model (RegCM2), I, Boundary-layer and radiative transfer processes, *Mon. Weather Rev., 121*, 2794-2813, 1993b.

Giorgi, F., M. R. Marinucci, and G. T. Bates, Development of a second-generation regional climate model (RegCM2), II, Convective processes and assimilation of lateral boundary conditions, *Mon Weather Rev., 121*, 2814-2832, 1993c.

Giorgi, F., C. Shields Brodeur, and G T Bates, Regional climate change scenarios over the United States produced with a nested regional climate model, *J. Clim., 7*, 375-399, 1994.

Grell, G. A., Prognostic evaluation of assumptions used by cumulus parameterizations, *Mon. Weather Rev., 121*, 764-787, 1993.

Hirakuchi, H., and F. Giorgi, Multiyear present-day and 2 x CO_2 simulations of monsoon climate over eastern Asia and Japan with a regional climate model nested in a general circulation model, *J. Geophys. Res., 100*, 21105-21125, 1995.

Holtslag, A. A. M., E. I. F. de Bruin, and H. L. Pan, A high resolution air mass transformation model for short-range weather forecasting, *Mon. Weather Rev., 118*, 1561-1575, 1990.

Hostetler, S. W., and P. J. Bartlein, Simulation of lake evaporation with application to modeling lake level variations of Harney-Malheur Lake, Oregon, *Water Resour. Res., 26*, 2603-2612, 1990.

Hostetler, S. W., G. T. Bates, and F. Giorgi, Interactive coupling of a lake thermal model with a regional climate model, *J. Geophys. Res., 98*, 5045-5057, 1993.

Jenkins, G., The 1988 and 1990 summer season simulations for west Africa using a regional climate model, *J. of Clim., 10*, 1255-1272, 1997.

Jenkins, G., and E. Barron, Global climate model and coupled regional climate model simulations over the eastern United States: GENESIS and RegCM2 simulations, *Global and Planet. Change 15*, 3-32, 1997.

Jones, R. G., J. M. Murphy, and M. Noguer, Simulation of climate change over Europe using a nested regional-climate model, I, Assessment of control climate, including sensitivity to location of lateral boundaries, *Q. J. R. Meteorol. Soc., 121*, 1413-1449, 1995.

Legates, D. R., and C. J. Willmott, Mean seasonal and spatial variability in gauge-corrected, global precipitation, *Int. J. Climatol., 10*, 111-127, 1990.

Liu, Y., R. Avissar and F. Giorgi, Simulation with the regional climate model RegCM2 of extremely anomalous precipitation during the 1991 east Asian flood: An evaluation study, *J. Geophys. Res. 101*, 26199-26215, 1996.

Luthi, D., A. Cress, C. Frei, and C. Schar, Interannual variability and regional climate simulations, *Theoret. Appl. Climatol., 53*, 185-206, 1996.

Lydolph, P. E., *Climates of the Soviet Union*, Elsevier Sci., New York, 1977.

Marinucci, M. R., and F. Giorgi, A 2xCO_2 climate change scenario over Europe generated using a limited area model nested in a general circulation model, 1, Present-day seasonal climate simulation, *J. Geophys. Res., 97*, 9989-10009, 1992.

Shukla, J., Dynamical predictability of monthly means, *J. Atmos. Sci., 38*, 2547-2572, 1981.

Small, E. E., S. Hostetler, L. C. Sloan, and F. Giorgi, Simulating the water balance of the Aral Sea with a coupled regional climate-lake model, *J. Geophys. Res.,* this issue.

Trenberth, K. E., Global analyses from ECMWF and atlas of 1000 to 10 mb circulation statistics, *NCAR Tech. Note, NCAR/TN-373+STR*, 191 pp, Natl. Cent. for Atmos. Res., Boulder, Colo., 1992.

Walsh, K , and J. McGregor, An assessment of simulations of climate variability over Australia with a limited area model, *Int. J. Climatol., 17*, 201-223, 1997.

F. Giorgi, National Center for Atmospheric Research, Boulder, CO 80307.

L. C. Sloan, and E. E. Small, Department of Earth Science, University of California Santa Cruz, 95064. (e-mail. lcsloan@es.ucsc.edu, esmall@es.ucsc.edu.)